Inherent Structure Landscape Connection between Liquids, Granular Materials, and the Jamming Phase Diagram

S. S. Ashwin,[1,2] Mahdi Zaeifi Yamchi,[1] and Richard K. Bowles[1]

[1]*Department of Chemistry, University of Saskatchewan, Saskatoon, Saskatchewan S7N 5C9, Canada*
[2]*Department of Mechanical Engineering and Material Science and Department of Physics,
Yale University, New Haven, Connecticut 06511, USA*

We provide a comprehensive picture of the jamming phase diagram by connecting the athermal, granular ensemble of jammed states and the equilibrium fluid through the inherent structure paradigm for a system of hard disks confined to a narrow channel. The J line is shown to be divided into packings that are either accessible or inaccessible from the equilibrium fluid. The J point itself is found to occur at the transition between these two sets of packings and is located at the maximum of the inherent structure distribution. We also present a general thermodynamic argument that suggests the density of the states at the maximum of the configurational entropy represents a lower bound on the J-point density in hard sphere systems. Finally, we show that the granular system, modeled using the Edwards ensemble, and the fluid sample the same set of thermodynamically accessible states over the full range of thermodynamic state points, but only occupy the same set of inherent structures, under the same thermodynamic conditions, at two points, corresponding to zero and infinite pressures, where they sample the J-point states and the most dense packing, respectively.

The physics of jamming [1–4] and how particles pack together influences the thermodynamic and mechanical properties of a variety of materials including crystals, liquids, glasses, and athermal granular materials. The problems encountered in the physics of jamming also have important overlaps with optimization problems in computer science [5] and information theory [6]. The jamming phase diagram [7,8], which locates the jamming transition as a function of various thermodynamic variables, was introduced in an attempt to describe the jamming phenomena of these systems within a unified conceptual framework. However, due to the complex nonequilibrium dynamics involved in any jamming protocol, establishing a clear relationship between the equilibrium fluid and the mechanically jammed states, remains a significant challenge [4].

Recent developments of the replica mean field theory (RMFT) [9–15], building on an earlier theory of the thermodynamic glass transition [16,17], have made significant advances in our understanding of the jamming phase diagram by studying a class of jammed matter that can be approximated as the infinite pressure glassy states of a liquid. By focusing on a region of the metastable liquid where the caging of the particles by their neighbors localizes their dynamics, RMFT employs a replica version of equilibrium liquid methodologies as a starting point and has been shown to successfully describe thermodynamics of this class of jammed states. Most importantly, the theory predicts that jamming, in some idealized models [18,19] and hard spheres [11,20], does not occur at a single transition J point, as originally suggested, but occurs over a set of points constituting a segment on the density axis referred to as the J line. The existence of the J line in the hard sphere model has been subsequently verified by simulations [21,22].

Within RMFT, the mean field relations describing the metastable state with volume fraction, ϕ, are mapped to relations describing the mechanically jammed states with volume fraction, ϕ_J, by considering a cage that momentarily traps the particles. The cage size is then systematically taken to zero under the mean field constraints. Physically, this amounts to an *artificial quench*, that renders the particles immobile due to their local neighborhood. The long lived glassy states first appear in the fluid at ϕ_d and artificially quenching these states locates the lowest density bound of the J line as ϕ_{th}. For hard spheres in three dimensions [10], $\phi_d \sim 0.58$, which coincides with the mode coupling density for the system, and $\phi_{th} \sim 0.64$. The upper bound of the J line, which occurs at the glass close packed density, ϕ_{GCP}, is obtained by artificially quenching the fluid at the Kauzmann density, ϕ_K, where the number of fluid states becomes subexponential and the system is expected to go through an ideal glass transition [23,24]. Again, for 3D hard spheres, RMFT finds ϕ_K and ϕ_{GCP} to be approximately 0.62 and 0.68, respectively. However, despite the success of RMFT, it does not capture the complete picture of jamming because the glassy states of the metastable fluid only represent a subset of all possible inherent structures [25–29], which are the mechanically stable packings formed from infinitely fast quenches of any equilibrium fluid configuration, at any ϕ. The density of the J point, ϕ_J^*, is defined as the ϕ_J of inherent

structures obtained from ideal gas configurations, and while many jamming protocols [8,30,31] do find $\phi_J^* \sim \phi_{th}$, such quenches are not accessible within RMFT. Other protocols [21,32] produce packing at much lower densities than 0.64 in hard spheres suggesting the existence of a wider range of packing densities than that predicted by RMFT.

In this Letter, we use a quasi-one-dimensional hard disk model, where the nonequilibrium dynamics of mapping fluid configurations to their inherent structures can be treated exactly for the full range of fluid densities, to explore the properties of the J line. We show the J line extends well below ϕ_{th} and can be divided into thermo-dynamically accessible and inaccessible jammed states. We also show that the J point locates the lowest density of thermodynamically accessible jammed states and is located at the maximum of the inherent structure distribution. Finally, we find that the granular system of this model, treated using the Edwards ensemble approach [33,34], samples the same set of thermodynamically accessible jammed states as the fluid, thus providing a fundamental link between these two states of matter.

We begin by generating the full ensemble of jammed states for a system of N, two-dimensional hard disks of diameter σ, confined to a narrow channel by two hard walls separated by a distance $H/\sigma < 1 + \sqrt{3/4}$. In D dimensions, a spherical particle is locally jammed if it has at least $D + 1$ rigid contacts arranged such that they are not all within the same hemisphere. However, the local jamming of all the particles in a structure is a necessary, but not sufficient, condition to ensure collective jamming because the concerted motion of a group of particles may allow the structure to collapse [35,36]. The confinement of the present model prevents the disks from passing each other, which eliminates the possibility of collective motions of particles unjamming the packings and allows us to count all the collectively jammed structures by simply consider-ing local packing constraints. It also ensures that each disk can only interact with its nearest neighbors and the wall. As a result, there are only four particle configurations that satisfy the local jamming constraints, two dense configu-rations (denoted 1 and 3) and two open, defect-type con-figurations, denoted 2 and 4 (see Fig. 1). The volume associated with each configuration is given by Hl_{ij}, where the l_{ij} is the longitudinal distance between neighboring disk centers, with $L_0 = l_{i,1} = l_{i,3} = [H(2\sigma - H)]^{1/2}$ and $l_{i,2} = l_{i,4} = \sigma$. Any jammed configuration can now be identified by an ordered list of compatible neighboring bonds [37]. However, some bond configurations are incom-patible in that they lead to unjammed configurations. For example, configurations containing neighboring defects, such as —2—2— or —4—4—, are not allowed as the central disk in the local arrangement is unjammed. All the jammed states of the model are isostatic [38]. Using the Edwards postulate that jammed states of equal volume are equally probable [33,34,38], we use the transfer matrix
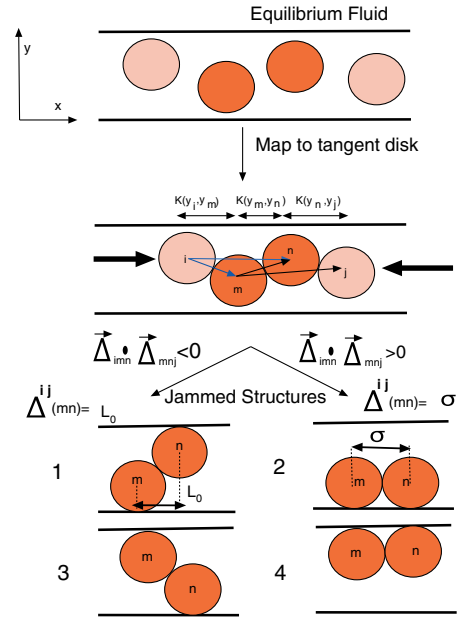

FIG. 1 (color online). Analytical quench connecting equilib-rium fluid configurations of disks i, m, n, j to the most dense (1, 3) and least dense (2, 4) local packing arrangements. Equilibrium configuration of four disks are initially mapped to a tangent disk configuration by compression in the x axis. The local arrangement of the disks contained in the product of the kernel $K(y_i, y_j)$ and the dot product of vectors [Eq. (4)] maps the central disks to their jammed configuration. See text for more details.

approach to study the ensemble of jammed states [37]. For a fixed N, the volume of the system will fluctuate depe-nding on the number of type 2 and 4 states in the configu-ration so we introduce a longitudinal pressure P_L, as a conjugate to the volume, and fix the system at a constant temperature, T. The transfer matrix is of the form: $M_{ij} = C_{ij} \exp(-\beta P_L h_0 l_{ij})$, where $h_0 = H - \sigma$. The exponential term is the Gibbs measure appropriate for the N, P_L, T ensemble and C_{ij} is zero when the two bonds are incom-patible [39] and one otherwise. $\beta = 1/kT$, where k is the equivalent to the Boltzmann constant in the jammed en-semble. In the thermodynamic limit, the partition function for the system is given by $\Delta(N, P_L, T) = NkT \ln(\lambda)$, where λ is the largest eigenvalue of M. ϕ_J and the configurational entropy, which is directly related to the number of jammed packings, $N_J(\phi_J)$, through $S_c = k \ln[N_J(\phi_J)]$, are given by

$$\phi_J = \frac{N\pi\sigma^2}{4HL_J} = -\frac{\pi\sigma^2}{4kT\partial(\ln\lambda)/\partial P_L}, \tag{1}$$

$$S_c/Nk = \ln\lambda + T\partial(\ln\lambda)/\partial T. \tag{2}$$

Figure 2 shows S_c/Nk as a function of ϕ_J for the case when $H/\sigma = 1.866$, obtained from a parametric plot of Eqs. (1) and (2) with respect to P_L. The same distribu-tion of states for this system can be obtained using a combinatorial approach [40]. The advantage of the present
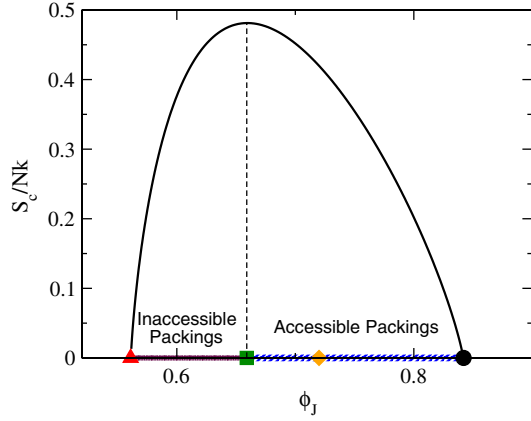
FIG. 2 (color online). S_c/Nk versus ϕ_J for $H/\sigma = 1.866$ showing features of the J line. The thermodynamically accessible packings have densities between the J point, with $\phi_J^* = 0.659$ (green square) and the most dense jammed state (black circle) with $\phi_J = 0.842$. $\phi_{th} \sim 0.72$ (orange diamond) is located at a higher density than the J point. The thermodynamically inaccessible packings densities between the J point and the least dense state with $\phi_J = 0.561$ (red triangle).

method is that it allows us to follow how the granular system explores the packing landscape as a function of the externally applied pressure and we have plotted the full equation of state (EOS) in Fig. 3. While there is no internal pressure from the particles in a granular system, it is still necessary for it to do work against P_L if the system expands to sample less dense states, but there are more low density basins than high density basins, so the balance between these two competing elements results in the "equilibrium" condition for the granular system. In the limit that $P_L h_0 \rightarrow \infty$, $S_c/Nk \rightarrow 0$ as the system moves
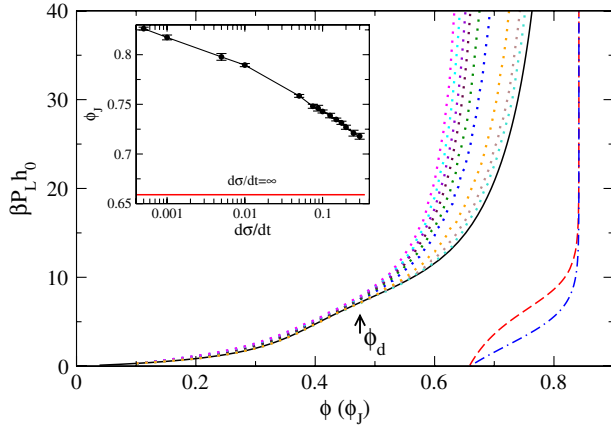

FIG. 3 (color online).   EOS for $H/\sigma = 1.866$. EOS for granular ensemble: $\beta P_L h_0$ as a function of ϕ_J (blue dot-dashed line). EOS for equilibrium thermal fluid: $\beta P_L h_0$ as a function of ϕ (black solid line). ϕ_J of basins sampled by equilibrium fluid (red dashed line). EOS for fluid compressed using the LS method with different $\partial\sigma/\partial t$ (dotted lines). $\phi_d \approx 0.48$ obtained from MD simulations. Insert: ϕ_J as a function of $\partial\sigma/\partial t$.

toward the most dense state with $\phi_J = 0.842$, while as $P_L h_0 \rightarrow 0$, the system samples the jammed states associated with the maximum in S_c where $\phi_J = 0.659$. If we use pressures below zero, we find less dense packings and the system enters the least dense jammed state with $\phi_J = 0.561$, $S_c/Nk = 0$, as $P_L h_0 \rightarrow -\infty$. However, there is no attraction between hard particles that could sustain a negative pressure, suggesting the packings below the S_c maximum are thermodynamically inaccessible.

We now examine how the equilibrium fluid for this system samples the landscape. The exact partition function for this model was originally solved by Barker [41], but we make use of the transfer matrix solution by Kofke *et al.* [42]. If the positions of the disks are fixed in the y direction, the configurational integral in the x direction can be simply treated as a Tonks gas [43]. Using a Laplace transform, the volume dependence is removed and the partition function, Z, in the N, P, T ensemble becomes

$$Z = \frac{1}{\Lambda^{DN}(\beta P_L)^{N+1}} \int dy K^N(y, y). \tag{3}$$

Here Λ is the thermal wavelength and $K(y_1, y_2) = \exp[-P_L h_0 L_x(y_1, y_2)]$, with y_1 and y_2 being the y coordinates of two adjacent disks in contact. L_x is the projection of the distance between the two contacting disks along the x axis and is a function of y_1, y_2. Solving the eigenvalue problem associated with Eq. (3) [42] yields the equilibrium EOS for the fluid plotted in Fig. 3. To quench the equilibrium fluid to its inherent structure, we take advantage of the information contained within the matrix K regarding the geometry of adjacent tangent disks. Starting from an equilibrium configuration, we translate the disks along the x axis only, so that the disks are in contact with their nearest neighbors. Figure 1 shows that the type of bond (1, 3 or 2, 4) between the two central disks (mn) that will result from further compression can be determined from the sign of the product of areas made from the triangles created by particles i, m, n and m, n, j. The geometry of the four disks is contained in the chain product matrix $K(y_i, y_m)K(y_m, y_n)K(y_n, y_j)$. The product *area-vector-product* rule, for triangles $\vec{\triangle}_{imn}$ and $\vec{\triangle}_{mnj}$, that determine the nature of the bond is

$$\begin{aligned} \vec{\triangle}_{imn} \bullet \vec{\triangle}_{mnj} > 0 \quad & \text{bond mn } \Delta_x^{ij}(mn) = l_{k,1} \\ \vec{\triangle}_{imn} \bullet \vec{\triangle}_{mnj} < 0 \quad & \text{bond mn } \Delta_x^{ij}(mn) = \sigma. \end{aligned} \tag{4}$$

We can now define a new transfer matrix G, whose elements are weighted by the bonds they would jam to under the jamming criterion, $G(i_2, i_3) = \sum_{i=i_1,i_4} K(i_1, i_2) \times K(i_2, i_3)K(i_3, i_4) \exp[\gamma\Delta_x^{ij}(mn)]$. For a system with periodic boundary conditions and $N - 2$ particles, the volume is given by $V_{N-2}^{inh} = \lim_{\gamma \rightarrow 0} \partial \log[\text{Tr}(G)]/\partial\gamma$.

This method represents an ideal, infinitely fast, non-equilibrium quench of the liquid to its inherent structure and amounts to a Stillinger map [27], where every

configuration is mapped uniquely to the jammed state of the inherent structure basin. Consequently, the probability of sampling a jammed state is weighted by the volume of configuration space in the inherent structure basin. Figure 3 shows both the equilibrium EOS for the fluid as a function of ϕ and the ϕ_J of the inherent structure sampled by the fluid. Both the fluid and the granular system sample the same set of thermodynamically accessible jammed states over the full range of thermodynamic state points, but the equilibrium properties of the fluid arise from competition between the configurational entropy (the number of basins) and the free volume of a single basin, while the granular ensemble has no free volume contribution. As a result, the fluid samples the inherent structure basins of jammed structures with a lower ϕ_J than the granular system, at the same pressure. However, the fluid and the granular system sample the same set of basins at two particular values of P_L. In the limit that $P_L \rightarrow \infty$, they both move toward the most dense state. There is only a single most dense structure, so the configurational entropy goes to zero, but there is no ideal glass transition in the fluid as this only occurs at $P_L \rightarrow \infty$ [44–46]. The two systems also sample the basins associated with the maximum in S_c as $P_L \rightarrow 0$, i.e., as the fluid approaches the ideal gas state.

A simple thermodynamic argument can help us understand which jammed states are thermodynamically accessible in hard sphere systems in general. The entropy of a hard particle fluid at ϕ is $S_f(\phi)/Nk = \ln N_g(\phi_J) + \ln Q_g(\phi, \phi_J)$, where $Q_g(\phi, \phi_J)$ is the configuration space of a single inherent structure basin that maps to ϕ_J. At equilibrium, the system samples the set of basins with ϕ_J that satisfy,

$$(\partial S_f/\partial \phi_J)_\phi = 0. \tag{5}$$

The free volume EOS [47] and the EOS for constrained glasses [28,29] suggest that $[\partial Q_g(\phi, \phi_J)/\partial \phi_J]_\phi \gtrless 0$. On the other hand, we generally expect there to be a single maximum in $N_g(\phi_J)$, with only a few very high or very low density states, because of the coupling between density and structural order [31] and estimates of hard sphere packing distributions generally yield a Gaussian distribution [28,29]. Combined, these conditions necessarily imply the equilibrium system is unable to sample basins with a ϕ_J lower than those at the S_c maximum. If the system did sample states with ϕ_J lower than the maximum, we would have $[\partial N_g(\phi_J)/\partial \phi_J] > 0$ and the equilibrium condition could never be satisfied. In addition, if the ideal gas does sample the basins associated with the S_c maximum, then $[\partial Q_g(\phi, \phi_J)/\partial \phi_J]_\phi = 0$, which suggests that the configurational volume of the basins, for all the glasses, becomes the same in the low density limit. This is true for the quasi-one-dimensional system studied here, and for the one-dimensional system of nonadditive hard rods, where at $\phi = 0$, all the particles in every glass become points caged

by their two neighboring points on the line. Speedy [48] found, for a binary mixture of hard disks in two dimensions, that the difference in entropy between the free ideal gas and the ideal gas constrained to a single basin is independent of the basin's ϕ_J. However, a recent study [49] of disk packings involving a small number of particles suggests that individual packings have geometry dependent basin volumes. Nevertheless, Eq. (5), in the limit $\phi \rightarrow 0$, defines the lowest density jammed packing accessible to the equilibrium fluid. This provides a thermodynamic definition of the J point.

We now use molecular dynamics simulations of our systems with $N = 10^4$ disks to compare our exact mapping scheme with a more traditional compression algorithm. Starting from a random, low density configuration with $\phi = 0.05$, the disks were compressed at a rate of $d\sigma/dt$ using a modified Lubachevsky and Stillinger [50] scheme that ensures H/σ remains constant as the disks are expanded. The EOS for the system under different compression rates are plotted in Fig. 3. The compressions follow the equilibrium EOS at low densities because the compression scheme allows the system to move between basins as it evolves. Eventually the fluid falls out of equilibrium at higher densities when caging effects start to become important and the system becomes trapped in a glassy state consisting of a single basin on the inherent structure landscape. Continued compression leads to a jammed state where the pressure diverges. The jamming density of the glasses, as a function of compression rate (see insert in Fig. 3), was obtained by counting the number of defects in the glass and taking averages over 20 independent runs at each $d\sigma/dt$. Not surprisingly, the jamming density increases with decreasing $d\sigma/dt$ as slower compression rates allow the system to remain in equilibrium longer. To reach the most dense state, the system must be compressed slowly enough to ensure that it remains in equilibrium at all points along the trajectory. The density at which the system first starts to fall out of equilibrium as a result of compression (see Fig. 3) provides us with an estimate of ϕ_d for our model. Packings generated from fluid configurations at this density give $\phi_{th} \sim 0.72$, but our exact results show that there are many more jammed configurations with a lower ϕ_J.

The details of particle packing in higher dimensions are significantly more complex than found in our model. Nevertheless, the simplicity of this system allows us to bring together many of the key elements of jamming, connecting jammed states with the equilibrium fluid and making a direct comparison of fluid and granular ensembles, to provide a comprehensive picture of the jamming phase diagram that has not been possible in higher dimensions. Our model also shares many of the same features of the jamming phase diagram of higher dimensions, such as a well-defined ϕ_d and a distribution of jammed structures that was speculated to exist by Ciamarra et al. [20] for

hard spheres. These common features suggest there is a strong possibility that the new details of the jamming phase diagram established here are also relevant to other hard particle systems.

[1] A. Coniglio, A. Fierro, H. J. Herrmannand, and M. Nicodemi, *Unifying Concepts in Granular Media and Glasses* (Elsevier, Amsterdam, 2004).

[2] M. van Hecke, J. Phys. Condens. Matter **22**, 033101 (2010).

[3] S. Torquato and F. H. Stillinger, Rev. Mod. Phys. **82**, 2633 (2010).

[4] M. Ciamarra, M. Nicodemi, and A. Coniglio, Soft Matter **6**, 2871 (2010).

[5] M. Mezard and A. Montanari, *Information, Physics, and Computation* (Oxford University, New York, 2009).

[6] C. A. Rogers, *Packing and Covering* (Cambridge University Press, Cambridge, England, 1964).

[7] A. J. Liu, and S. R. Nagel, Nature (London) **396**, 21 (1998).

[8] C. S. O'Hern, S. A. Langer, A. J. Liu, and S. R. Nagel, Phys. Rev. Lett. **88**, 075507 (2002); C. S. O'Hern, L. E. Silbert, A. J. Liu, and S. R. Nagel, Phys. Rev. E **68**, 011306 (2003).

[9] G. Parisi and F. Zamponi, J. Chem. Phys. **123**, 144501 (2005).

[10] F. Zamponi, Philos. Mag. **87**, 485 (2007).

[11] G. Parisi and F. Zamponi, Rev. Mod. Phys. **82**, 789 (2010).

[12] I. Biazzo, F. Caltagirone, G. Parisi, and F. Zamponi, Phys. Rev. Lett. **102**, 195701 (2009).

[13] L. Berthier, H. Jacquin, and F. Zamponi, J. Stat. Mech. (2011) P01004.

[14] H. Jacquin, L. Berthier, and F. Zamponi, Phys. Rev. Lett. **106**, 135702 (2011).

[15] L. Berthier, H. Jacquin, and F. Zamponi, Phys. Rev. E **84**, 051103 (2011).

[16] M. Mezard and G. Parisi, Phys. Rev. Lett. **82**, 747 (1999).

[17] M. Mezard and G. Parisi, J. Chem. Phys. **111**, 1076 (1999).

[18] F. Krzakala and J. Kurchan, Phys. Rev. E **76**, 021122 (2007).

[19] R. Mari, F. Krzakala, and J. Kurchan, Phys. Rev. Lett. **103**, 025701 (2009).

[20] M. Pica Ciamarra, A. Coniglio, and A. De Candia, Soft Matter **6**, 2975 (2010).

[21] P. Chaudhuri, L. Berthier, and S. Sastry, Phys. Rev. Lett. **104**, 165701 (2010).

[22] C. F. Schreck, C. S. O'Hern, and L. E. Silbert, Phys. Rev. E **84**, 011305 (2011).

[23] P. G. Debenedetti and F. H. Stillinger, Nature (London) **410**, 259 (2001).

[24] C. A. Angell, J. Res. Natl. Inst. Stand. Technol. **102**, 171 (1997).

[25] M. Goldstein, J. Chem. Phys. **51**, 3728 (1969).

[26] F. H. Stillinger, E. DiMarzio, and R. L. Kornegay, J. Chem. Phys. **40**, 1564 (1964).

[27] F. H. Stillinger and T. A. Weber, Phys. Rev. A **25**, 978 (1982).

[28] R. J. Speedy, Mol. Phys. **95**, 169 (1998).

[29] R. J. Speedy, J. Chem. Phys. **114**, 9069 (2001).

[30] T. M. Truskett, S. Torquato, and P. G. Debenedetti, Phys. Rev. E **62**, 993 (2000).

[31] S. Torquato, T. M. Truskett, and P. G. Debenedetti, Phys. Rev. Lett. **84**, 2064 (2000).

[32] Y. Jiao, F. H. Stillinger, and S. Torquato, J. Appl. Phys. **109**, 013508 (2011).

[33] S. F. Edwards and R. B. S. Oakeshott, Physica (Amsterdam) **157**, 1080 (1989).

[34] S. F. Edwards and D. V. Grinev, Phys. Rev. E **58**, 4758 (1998).

[35] S. Torquato and F. H. Stillinger, J. Phys. Chem. B **105**, 11849 (2001).

[36] A. Donev, F. H. Stillinger, and S. Torquato, Phys. Rev. Lett. **95**, 090604 (2005).

[37] S. S. Ashwin and R. K. Bowles, Phys. Rev. Lett. **102**, 235701 (2009).

[38] R. K. Bowles and S. S. Ashwin, Phys. Rev. E **83**, 031302 (2011).

[39] $\{i, j\} = \{1, 1\}, \{1, 4\}, \{2, 1\}, \{2, 2\}, \{2, 4\}, \{3, 2\}, \{3, 3\}, \{4, 2\}, \{4, 4\}$.

[40] R. K. Bowles and I. Saika-Voivod, Phys. Rev. E **73**, 011503 (2006).

[41] J. A. Barker, Aust. J. Phys. **15**, 127 (1962).

[42] D. A. Kofke and A. J. Post, J. Chem. Phys. **98**, 4853 (1993).

[43] L. Tonks, Phys. Rev. **50**, 955 (1936).

[44] A. Donev, F. H. Stillinger, and S. Torquato, Phys. Rev. Lett. **96**, 225502 (2006).

[45] S. L. Simon and G. B. McKenna, J. Non-Cryst. Solids **355**, 672 (2009).

[46] M. Z. Yamchi, S. S. Ashwin, and R. K. Bowles, Phys. Rev. Lett. **109**, 225701 (2012).

[47] A. Donev, S. Torquato, and F. H. Stillinger, Phys. Rev. E **71**, 011105 (2005).

[48] R. J. Speedy, J. Mol. Struct. **485**, 537 (1999).

[49] S. S. Ashwin, J. Blawzdziewicz, C. S. O'Hern, and M. D. Shattuck, Phys. Rev. E **85**, 061307 (2012).

[50] B. D. Lubachevsky and F. H. Stillinger, J. Stat. Phys. **60**, 561 (1990).